Prepared for submission to JCAP

Ubiquity of density slope oscillations in the central regions of galaxy and cluster-sized systems

Anthony M. Young[1] , **Liliya L. R. Williams**[1] , **and Jens Hjorth** [2]

[1]School of Physics and Astronomy, University of Minnesota, 116 Church Street SE, Minneapolis, MN 55455, USA

[2]Dark Cosmology Centre, Niels Bohr Institute, University of Copenhagen, Juliane Maries Vej 30, DK-2100 Copenhagen, Denmark

E-mail: amyoung@astro.umn.edu,llrw@astro.umn.edu,jens@dark-cosmology.dk

Abstract. One usually thinks of a radial density profile as having a monotonically changing logarithmic slope, such as in NFW or Einasto profiles. However, in two different classes of commonly used systems, this is often not the case. These classes exhibit non-monotonic changes in their density profile slopes which we call oscillations for short. We analyze these two unrelated classes separately. Class 1 consists of systems that have density oscillations and that are defined through their distribution function $f(E)$, or differential energy distribution $N(E)$, such as isothermal spheres, King profiles, or DARKexp, a theoretically derived model for relaxed collisionless systems. Systems defined through $f(E)$ or $N(E)$ generally have density slope oscillations. Class 1 system oscillations can be found at small, intermediate, or large radii but we focus on a limited set of Class 1 systems that have oscillations in the central regions, usually at $\log(r/r_{-2}) \lesssim -2$, where r_{-2} is the largest radius where $d\log(\rho)/d\log(r) = -2$. We show that the shape of their $N(E)$ can roughly predict the amplitude of oscillations. Class 2 systems which are a product of dynamical evolution, consist of observed and simulated galaxies and clusters, and pure dark matter halos. Oscillations in the density profile slope seem pervasive in the central regions of Class 2 systems. We argue that in these systems, slope oscillations are an indication that a system is not fully relaxed. We show that these oscillations can be reproduced by small modifications to $N(E)$ of DARKexp. These affect a small fraction of systems' mass and are confined to $\log(r/r_{-2}) \lesssim 0$. The size of these modifications serves as a potential diagnostic for quantifying how far a system is from being relaxed.

arXiv:1604.01409v1 [astro-ph.CO] 5 Apr 2016

Contents

1 Introduction **1**

2 DARKexp **5**

3 Class 1: Density Slope Oscillations in Systems Defined by $f(E)$ or $N(E)$ **5**

4 Class 2: Density Slope Oscillations in Dynamically Evolved Halos **11**
4.1 Numerically simulated systems 11
4.2 Observed systems 13

5 Conclusions **16**

1 Introduction

The distribution of dark matter in galaxies and clusters of galaxies is well described by ΛCDM numerical N-body simulations of cosmological structure formation and evolution. These simulations produce near universal dark matter halo radial density profiles over a few decades in radius [1, 2]. In general, the Navarro-Frenk-White (NFW) profile [3] provides a good fit to density profiles of equilibrium dark matter halos [4–10]. However, there are some discrepancies between simulations and observations. For example, the core/cusp problem [11]: N-Body simulations produce cuspy central density profiles [12], well fit by the NFW profile, while some observations show core like centers in dark matter dominated systems, like dwarf galaxies [13, 14].

In this paper, we concentrate on an aspect absent from NFW and other phenomenological models. A close inspection shows that at small radii, both observations and high resolution simulations often exhibit oscillatory behavior in radial, total mass density profiles. Though we call them oscillations, no time evolution is implied, these are time-stationary features. Within simulations, this can be seen in the dark matter galactic evolution simulations GHALO and Via Lactea 2, as well as dark matter plus hydrodynamics simulations [15, 16]. Nuclear star cluster also represent oscillations in density within the host galaxy [17, 18]. Observational data presented by Newman et al. [19] of galaxy clusters, Sloan Digital Sky Survey (SDSS) elliptical galaxies presented by Chae et al. [20], and density profiles of luminous red galaxies based on satellite kinematics [21] show oscillations in their central regions. For example, Figure 1 shows the density profiles of seven equilibrium galaxy clusters presented in Newman et al. [19]. The density slope interior to $\log(r/r_{-2}) \sim 0$ is changing non-monotonically, i.e. oscillating. The x-axis is normalized by the largest radius value where the density slope is $\gamma = 2$, where $\gamma = -d\log\rho/d\log r$, and is called r_{-2}. The r_{-2} convention is used, since in some systems, like DARKexp, the virial radius is not defined [22]. The Newman et al. profiles are built from strong and weak gravitational lensing observations along with resolved stellar kinematics within the bright central galaxies to produce the radial density profiles that include both dark and baryonic matter. Their profiles consist of two main components: the dark matter halo and the stars in the bright central galaxy. For the dark matter halo, a generalized NFW (gNFW) profile is used, which gives the profile its $\gamma = 3$ large radii behavior.

Class 1 Systems	
DARKexp profiles [23]	$N(\epsilon) = A[e^{\phi_0 - \epsilon} - 1]$
Polytrope [24, 25]	$f(\epsilon) = A\epsilon^{n-3/2}, \quad n = 5 \pm \eta \quad (\eta << 1), \quad n > 5$
Isothermal Sphere (IS) [26]	$f(\epsilon) = \frac{\rho_0}{(2\pi\sigma^2)^{3/2}} e^{\epsilon/\sigma^2}$
Lowered Isothermal Models [27]	$f(E, J^2) = A \exp\left(-\frac{J^2}{2r_a^2 s^2}\right) E_\gamma\left(g, -\frac{E - \phi(r_t)}{s^2}\right)$
King profiles [28]	$f(\epsilon) = \rho_1 (2\pi\sigma^2)^{-3/2} (\exp(\epsilon/\sigma^2) - 1)$
Class 2 Systems	
SDSS elliptical galaxies [20]	
Massive galaxy clusters [19]	
GHALO$_2^1$ ($\epsilon = 61.0pc$) [2]	
Via Lactea 2^1($\epsilon = 40.0pc$) [16]	
EAGLE^2 ($\epsilon = 700pc$) [29]	
Non Oscillating Systems	
Hernquist profiles [30]	$\rho(r) = \frac{M}{2\pi} \frac{a}{r} \frac{1}{(r+a)^3}$
Polytrope [24, 25]	$\rho(r) = \rho_c \Psi^n$ e.g. $\Psi_0 = 1 - r^2/6, \quad \Psi_1 = \frac{\sin r}{r}, \quad \Psi_5 = (1 + \frac{1}{3} r^2)^{-1/2}$
NFW and gNFW profiles [3]	$\rho(r) = \frac{\rho_s}{(r/r_s)^\alpha (1 + r/r_s)^{3-\alpha}}$
Einasto profiles [31]	$\rho(r) = \rho_s \exp\{-b_n[(r/r_s)^{1/n} - 1]\}$
Navarro et al. [1] profiles^{1,2}	
Millennium-II^2 ($\epsilon = 1370pc$) [32]	
Aquarius^2(AQ-1 $\epsilon = 20.5pc$) [33]	

Table 1. An incomplete list of density profiles. Class 1 systems consist of systems defined through a physics based approach that have density slope oscillations. Class 2 systems are dynamically evolved systems with density slope oscillations. Note that polytropic models can produce oscillations or no oscillations in density slope depending on the polytropic index, n. A raised 1 indicates the base code is PKDGRAV while a raised 2 indicates GADGET. EAGLE also includes hydrodynamics to account for baryonic effects. Equations for distribution functions or differential energy distributions and density profiles are given when appropriate.

The origins of oscillations in density profiles of equilibrium systems have not been investigated in depth. Density profiles that are monotonic in logarithmic density slope by construction, like NFW and Einasto [31], are able to capture the general shape of halo density curves but do not capture the oscillation features in density at small radii.

Just like baryonic effects can be used to transform density cusps into cores [34–42] in the central regions of dwarfs, they can also be used as part of an explanation for the origins of oscillations in density profiles. As baryons cool, they condense to the centers of halos which can further pull dark matter to centrally concentrate it [43]. Other baryonic effects, like feedback, can decrease the central concentrations in halos. All these effects change the dark matter and total matter configuration when compared to dark matter only systems. Hydrodynamic codes have been added to structure formation simulations to account for the competing baryonic effects on mass [39, 44–53]. The combination of these baryonic effects and the response of the dark matter usually leads to a net increase in the central mass density in clusters and early type galaxies, thereby producing oscillatory features in central regions. These oscillations are better described by their slopes and we will refer to density slope oscillations from now on.

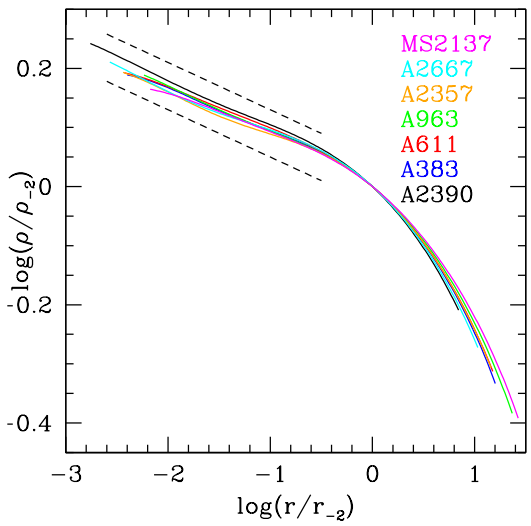

Figure 1. Density profiles for seven massive, equilibrium galaxy clusters presented in Newman et al. [19]. The density oscillations are the deviations from a monotonically changing slope in the region $\log(r/r_{-2}) < 0$. The x-axis is normalized by the radius value where the density slope is $\gamma = 2$ and is called r_{-2}. The y-axis is normalized by the value of the density at $\gamma = 2$, and is called ρ_{-2}. The dashed parallel lines serve as guidelines to better find the oscillations and highlight the region of interest.

However, this explanation in terms of baryons is not completely satisfactory. It does not explain why relaxation following, for example a merger, or central galaxy formation, or some other formation event within a cluster, does not fully incorporate the central cluster galaxy into the rest of the cluster. In other words, why the change in the density slope which marks the transition in radius between the central galaxy and cluster remains easily identifiable and does not get erased by relaxation. The same statement can be made about the central regions of galaxies that exhibit an upturn in the mass density. The persistence of this visible transition implies that the relaxation in the central parts is incomplete.

In this paper we will not address the physical reasons behind incomplete relaxation; instead, we will provide support for the incomplete relaxation interpretation of the density slope oscillations, through two lines of argument. First, we will show that the differential energy distributions of the oscillating density slope systems deviate only slightly, and in a simple way from those of fully relaxed systems, namely DARKexp. Second, we will show that similar, but smaller amplitude slope oscillations are also present in some high resolution pure dark matter simulated halos, and that these have differential energy distributions that differ from that of DARKexp in a similar way to the observed systems described above. Note that baryonic effects cannot be invoked to explain oscillating density features in these simulations, underscoring that baryons do not provide the full explanation in observed systems either. To put it differently, we argue that density slope oscillations seen in observed systems and pure dark matter simulations have a common origin: both are indicators that the central regions of these systems, though in stable equilibrium, are not fully relaxed. A fully relaxed system does not contain any information about its past history and assembly, and so should

look similar to DARKexp, which does not have density slope oscillations in the radial range $-2 < \log(r/r_{-2}) < 0$.

We call the observed and simulated systems discussed in the last three paragraphs dynamically evolved, because that is how they arrived at their present state, through dynamical evolution to reach their present, near steady-state configuration. Our analysis related to them (Class 2 systems) is presented in Section 4. However, we start our discussion of density slope oscillations in Section 3 by addressing a very different set of density profile models; those that were arrived at through a mathematically formulated physics-based argument or principle which we call Class 1 systems. Examples include isothermal spheres, DARKexp, and polytropes. The reasons for these exhibiting density slope oscillations is different than the dynamically evolved systems mentioned above.

These physics-based models start as derivations or arguments in terms of $f(E)$ or $N(E)$, i.e. quantities that involve the full dynamics, and not just the configuration space: these are never started as density profiles. It appears that monotonic shapes in $f(E)$ and $N(E)$ generically lead to non-monotonic $\gamma(r)$ for these systems. This is unlike phenomenological density slope profiles that are monotonically changing in log space by construction and contain parameter(s) that are optimized by fitting to the density profiles. These do not have any density slope oscillations by design. We recognize that there are exceptions to our classification. For example, polytrope of $n = 5$ (Plummer sphere), whose density profile slope does not oscillate is a physics-based system. Exceptions notwithstanding, our goal is to show that oscillations in physics-based models are not an unusual occurrence.

A non-exhaustive list of different models and data with oscillating and non-oscillating density profile slopes is presented in Table 1. For simulations, the basic source code is identified and the softening parameter is listed. Note that for the simulation profiles with oscillations listed, the oscillations happen at radii larger than the softening parameter. Equations for the differential energy distribution or the distribution functions of Class 1 systems and for density profiles in the non-oscillating list are given when appropriate. The density profiles of non-oscillating systems in Table 1 do not have simple analytic expressions for their f(E) and N(E), with the exception of polytropes. Likewise, Class 1 systems usually don't have analytic expressions for their density profiles.

While these profiles are spherically symmetric, it is important to note that actual systems could look different in three dimensions, they could have some ellipticity and substructure. Ellipticity means that there are density anisotropies along certain radial directions. Radial perturbations do not map to oscillations because the latter are tangential perturbations in the density profile. We discuss substructure at the beginning of Section 4.

To summarize, not all density slope oscillations are the same; we identify two classes of systems that possess density slope oscillations: Class 1 are the ones seen in physical argument based models that appear to exist because most $f(E)$ and $N(E)$ lead to density profiles with non-monotonic slopes, while Class 2 systems are the ones seen in dynamically evolved systems that are likely to arise from incomplete relaxation. The two causes of oscillations seem to be unrelated, and so can be "superimposed" in a single system. Furthermore, as we discuss in the following Sections, the two classes of oscillations affect different radial ranges in the density profiles, so they can be easily distinguished.

In Section 2, we describe the DARKexp distribution and its density profiles. In Section 3, we explore additional energy distributions that, while not being based on physical arguments, are defined through $f(E)$ or $N(E)$ and characterize the oscillations they produce. We then use DARKexp as a basis for fitting a model to observed and simulated density profiles in Section

4. Because Class 1 and 2 systems with density slope oscillations are unrelated, Sections 3 and 4 are largely independent of each other. We anticipate that Class 2 systems (Section 4) will be of more interest to most readers. We discuss our findings and conclude in Section 5.

2 DARKexp

DARKexp is a physics-based, equilibrium statistical mechanical theory of collisionless self-gravitating dark matter systems [23]. Its differential energy distribution is given by

$$N(\epsilon) \propto \exp(\phi_0 - \epsilon) - 1 \tag{2.1}$$

where ϕ_0 is the dimensionless central potential and ϵ is the dimensionless energy. ϕ_0 and ϵ can be related to Φ_0 and E, the potential energy and total energy respectively, as $\phi_0 = \beta\Phi_0$ and $\epsilon = \beta E$ by β, the inverse temperature.

The development of DARKexp is motivated by determining the origin of collisionless, self-gravitating structure. It follows similar statistical mechanics arguments as the derivation of Maxwell-Boltzmann distribution but deviates in two important ways. The first is that the system is described in total orbital energy space instead of the traditional position and velocity 6-D phase space. This is because particles in a collisionless system retain their energy in contrast to those in collisional systems. The second point is that low occupancy numbers of the energy state space are treated more accurately with a better representation of $n!$ than the Stirling approximation.

While the energy distribution of DARKexp is analytically known, the resulting density profile must be calculated numerically through iteration [22, 54]. The DARKexp asymptotic density slope is -1 ($\gamma = 1$) as $r \to 0$ for all central potentials, but the slopes do not monotonically approach -1. See Figure 2, where we plot the density slope, γ. Depending on the central potential value, ϕ_0, DARKexp can recreate the density profile slope range ($0 \lesssim \gamma \lesssim 2$) seen in the above mentioned simulations and observations, at radii $-2 \lesssim \log(r/r_{-2}) \lesssim 0$. At these radii, DARKexp profiles that closely resemble physical systems (those with $2 \lesssim \phi_0 \lesssim 8$) do not exhibit slope oscillations while observed and simulated systems do; for example, see Figure 1.

Because the oscillations in DARKexp versus those in dynamically evolved systems occur at different radii, there is little chance of confusing them. This can be seen in Figure 3 where density slope profile of DARKexp with $\phi_0 = 4.0$ and data from the simulation Via Lactea 2 are plotted together. The Via Lactea 2 oscillations are in the radial range $-2 < \log r/r_{-2} < 0$. At radii smaller than $\log(r/r_{-2}) \sim -2$, DARKexp profiles begin to oscillate. However, these small radii are currently inaccessible to either observations or high resolution simulations. We will return to DARKexp oscillations in Section 3.

Presumably, the oscillations extend into smaller radii but the numerical resolution of the code that produced Figure 2 becomes the limiting factor and numerical effects start to dominate on average shortly after $\log(r/r_{-2}) \sim -4.5$, although this appears to be ϕ_0 and code resolution dependent.

Aside from center oscillating $\gamma(r)$, DARKexp closely resemble results of numerical simulations and observations [55–59] which do not extend much beyond $\log(r/r_{-2}) \sim -2.5$.

3 Class 1: Density Slope Oscillations in Systems Defined by $f(E)$ or $N(E)$

In this Section, we expand on our assertion that systems obtained from some physical argument, instead of being dynamically evolved, usually exhibit density slope oscillations. We

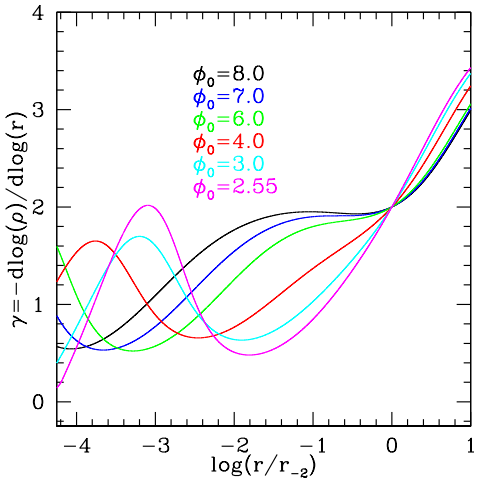

Figure 2. DARKexp density profile slopes for several central potentials. From top to bottom at $\log(r/r_{-2}) = -1$, the halo potential depths are $\phi_0 = 8.0, 7.0, 6.0, 4.0, 3.0, 2.55$. The horizontal axis is normalized to the radius, r_{-2}, where the density slope is $\gamma = 2$.

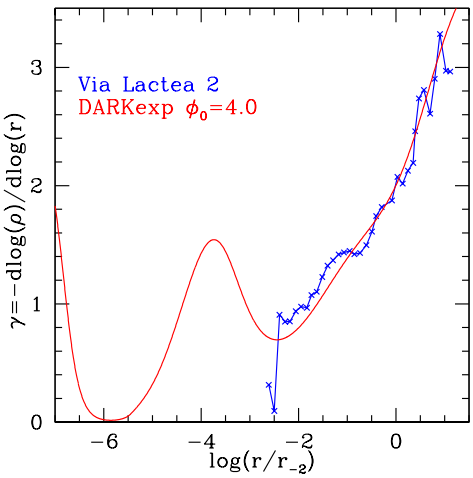

Figure 3. Density slope profile for DARKexp with $\phi_0 = 4.0$ and data from the simulation Via Lactea 2. Note the different amplitudes and radial regions where the oscillations are present. The Via Lactea 2 oscillations are in the radial range $-2 < \log r/r_{-2} < 0$.

also investigate if there is a link between the amplitude of oscillations in density profile slope and the shape of $N(E)$.

The key aspect of physics-based systems is that their mathematical description is always for $f(E)$ or $N(E)$, and never for the density profile. Examples are (see Table 1): isothermal spheres, whose $f(E)$ is an exponential in energy, and whose equation of hydrostatic equilibrium is the same as that of isothermal gas; polytropes, whose $f(E)$ is a power law in energy, and they represent self-gravitating spheres with a polytropic equation of state, and DARKexp, whose derivation is described in Section 2.

All above examples, as well as other examples of physics-based models have simple analytical expressions for either $f(E)$ or $N(E)$. This is their distinguishing feature. On the other hand, non physics-based models have either very complicated expressions for $f(E)$ or $N(E)$ because they were obtained from $\rho(r)$ (like Hernquist, 1990), or do not have analytical expressions at all (like NFW and Einasto).

While all the Class 1 systems in Table 1 oscillate, not all do so at small radii. Polytropes at n around 5 have density slope oscillations at large radii [25], while isothermal spheres have them at intermediate radii [26]. Because the model that represents relaxed collisionless systems, DARKexp, has oscillations at very small radii, we are mostly interested in small radius oscillations, and therefore we decided to use simple functional forms of $N(E)$ that produce density profiles which oscillate at small radii.

We chose two functional forms:

$$N(\epsilon) \propto (\phi_0 - \epsilon)^{1/\alpha} \tag{3.1}$$

and

$$N(\epsilon) \propto e^{\phi_0 - \epsilon}(\phi_0 - \epsilon)^{1/\alpha} \tag{3.2}$$

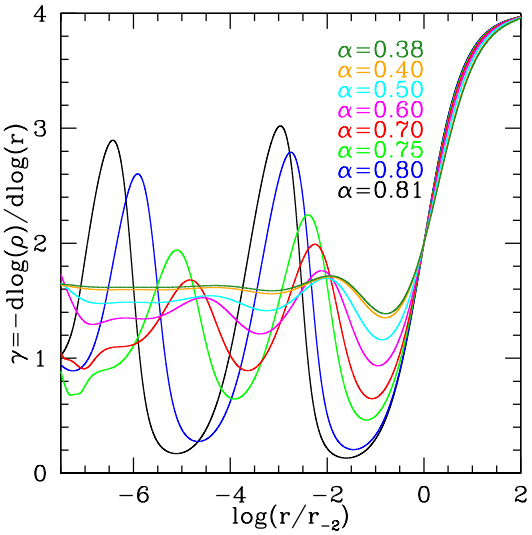

Figure 4. Density profile slopes created from energy distributions given by $N = (\phi_0 - \epsilon)^{1/\alpha}$ with $\phi_0 = 4.0$. The values of α span a range that provides numerical convergence in the code. The higher the value of α, the larger the oscillation in density profile. From top to bottom at $\log(r/r_{-2}) = -1$, $\alpha = 0.38, 0.40, 0.50, 0.60, 0.70, 0.75, 0.80, 0.81$. The asymptotic log-log density profile slope at small radii is given by $\gamma \propto 2 - \alpha$, which yields $\gamma_{asymp} = 1.62, 1.6, 1.5, 1.4, 1.3, 1.25, 1.2, 1.19$ for the previous list of α values, respectively. These values will define a baseline used for further comparisons.

where ϕ_0 is a dimensionless central potential found in DARKexp and α is a free parameter.

Though these $N(E)$ are not a result of a physical principle or argument, they share one key aspect with isothermal spheres, polytropes, and DARKexp: they are defined through simple expression of $f(E)$ or $N(E)$. We now show that for these systems, density slope oscillations are common and that the shape of $N(E)$ can approximately predict the "strength" of oscillations of the corresponding density profiles.

Two sample profile collections are shown in Figure 4 and Figure 5 and represent equation (3.1) and equation (3.2), respectively; both assume a central potential of $\phi_0 = 4.0$. The range of α values ensured convergence given the code's resolution in radius. For all the α values for each energy distribution, the density seems to oscillate about the expected small radii behavior given in Hjorth & Williams [23], which is $\rho \propto r^{\alpha-2}$, but with different amplitudes.

To quantitatively assess the density profiles, we created an oscillation parameter, κ. We will use κ to quantify oscillations as it gauges the difference between the profile slope and its asymptotic small radius behavior. Since $\rho \propto r^{\alpha-2}$, this would mean $\gamma \propto 2 - \alpha$ at small radii in log space. κ is defined as the enclosed area between the density profile slope, γ, and the requisite baseline $2 - \alpha$. κ was calculated over one complete oscillation for each α value. One oscillation is counted as crossing the small radius baseline two additional times starting from $\log(r/r_{-2}) = 0$ and can be seen in Figure 6 for DARKexp of several ϕ_0.

There are some limitations to using this area characterization. It may not accurately represent high frequency oscillations that could be defined as oscillating more than a low frequency oscillation with the same amplitude. Fortunately, we did not see any oscillations that had different frequencies but the same amplitude. The concept of frequency used here is

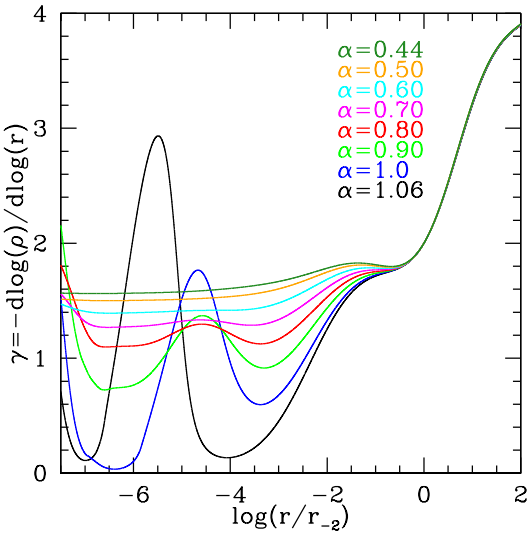

Figure 5. Density profile slopes created from energy distributions given by $N = e^{\phi_0 - \epsilon}(\phi_0 - \epsilon)^{1/\alpha}$ with $\phi_0 = 4.0$. The values of α span a range that provides numerical convergence in the code. The higher the value of α, the larger the oscillation in density profile. From top to bottom at $\log(r/r_{-2}) = -2$, $\alpha = 0.44, 0.50, 0.60, 0.70, 0.80, 0.90, 1.0, 1.06$. The asymptotic log-log density profile slope at small radii is given by $\gamma \propto 2 - \alpha$, which yields $\gamma = 1.56, 1.5, 1.4, 1.3, 1.2, 1.1, 1.0, 0.94$ for the previous list α values, respectively. These values will define a baseline used for further comparisons.

the measure of how often the peak in the oscillation is repeated per unit distance in $\log(r/r_{-2})$ space.

The curves in Figure 6 represent the result of the subtraction between the original γ profile and the asymptotic behavior for DARKexp profiles, which is $\rho \propto r^{-1}$, so $\gamma = 1$. The result is then integrated to find the area, κ; all area is considered positive.

Our aim is to relate the amplitude of density slope oscillations to the shape of the differential energy distribution. From visual examination, we noticed that $N(E)$ which are shallower (have smaller absolute values of $d\log(N)/d\epsilon$) close to the most binding energy tend to produce density profiles with higher slope oscillations. Trial and error showed that taking the slope of $N(E)$ at $\epsilon = 0.8\phi_0$ works well. Figure 7 plots the area under the curve, κ, against $d\log(N)/d\epsilon$ evaluated at $\epsilon = 0.8\phi_0$. The plotted curve shows that there is a relation between slope oscillations in $\rho(r)$ and $N(E)$, or that the shape of the energy distribution determines how much the density slope will oscillate.

We did the same analysis for the different functional families given by equation (3.1) and equation (3.2) with $\alpha = 1.05, 1.0, 0.8, 0.7, 0.5, 0.38$ and $\alpha = 0.81, 0.8, 0.75, 0.6, 0.5, 0.38$ respectively. κ for both of the two families with $\phi_0 = 4.0$ ($\phi_0 = 2.55$) are plotted as solid boxes in Figure 8 (Figure 9) as well as a red data point for DARKexp with the same ϕ_0. Across both families and both central potentials, κ increases as α increases. It appears that less negative slopes, $d\log(N)/d\epsilon$ (higher α), in energy density produce more area under the curve and therefore more oscillations in density profiles for these two distributions, by our metric.

From the fact that κ increases with increasing α, one might think that the oscillation

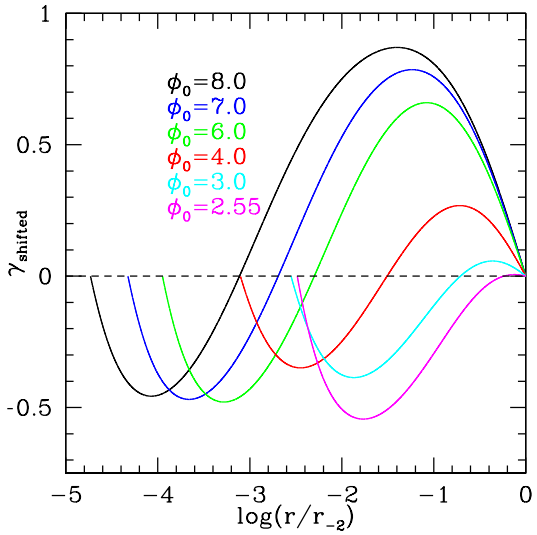

Figure 6. One oscillation of the density profile slopes from Figure 2 after their small radius asymptotic baseline has been subtracted which for DARKexp is $\rho \propto r^{-1}$. The positive area was calculated from these profiles. The term "positive area" means the absolute value was applied for the parts of the curve that would produce negative area. We called this area under one oscillation, κ. For reference, the black dashed line is $\gamma = 0$.

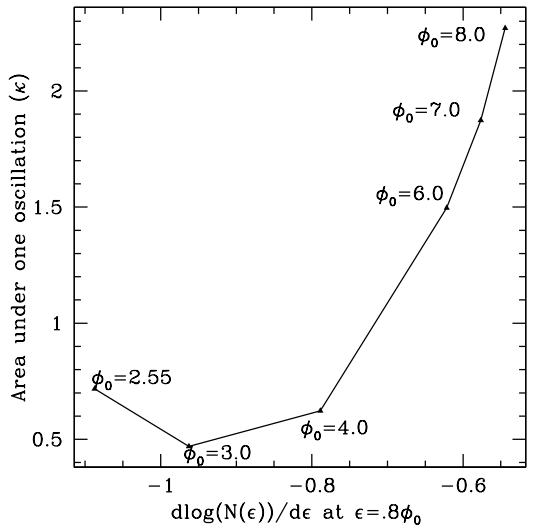

Figure 7. Area under the curve, κ, for one oscillation of DARKexp central potentials $\phi_0 = 8.0, 7.0, 6.0, 4.0, 3.0, 2.55$. The slope of the density profile had to be evaluated at a specific energy, so $\epsilon = 0.8\phi_0$ was arbitrarily chosen.

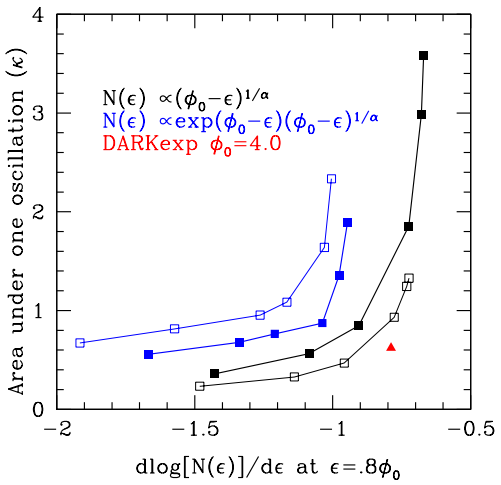

Figure 8. Area under the curve, κ, for one oscillation for $N = e^{\phi_0-\epsilon}(\phi_0-\epsilon)^{1/\alpha}$ and $N = (\phi_0-\epsilon)^{1/\alpha}$ with $\phi_0 = 4.0$. The different points represent the different α values with (from top to bottom) $\alpha = 1.05, 1.0, 0.8, 0.7, 0.5, 0.38$ for $N = e^{\phi_0-\epsilon}(\phi_0-\epsilon)^{1/\alpha}$ and with (from top to bottom) $\alpha = 0.81, 0.8, 0.75, 0.6, 0.5, 0.38$ for $N = (\phi_0-\epsilon)^{1/\alpha}$. Solid squares represent the original $N = e^{\phi_0-\epsilon}(\phi_0-\epsilon)^{1/\alpha}$ and $N = (\phi_0-\epsilon)^{1/\alpha}$ distributions and open squares represent the distributions modified to be $N_{new} = N(1+\mu(\phi_0-\epsilon)^v)$. DARKexp with $\phi_0 = 4.0$ is plotted as the red data point for reference.

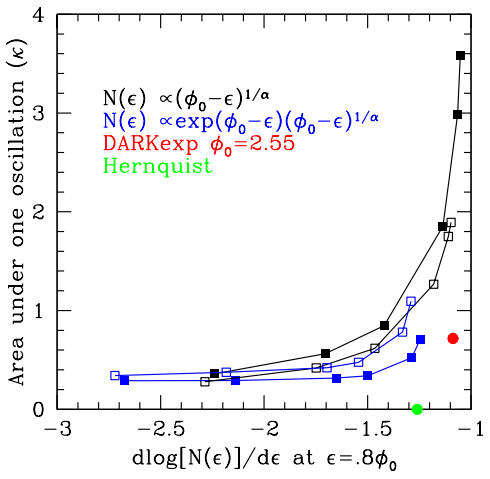

Figure 9. Area under the curve, κ, for one oscillation for $N = e^{\phi_0-\epsilon}(\phi_0-\epsilon)^{1/\alpha}$ and $N = (\phi_0-\epsilon)^{1/\alpha}$ with $\phi_0 = 2.55$. The different points represent the different α values with (from top to bottom) $\alpha = 1.05, 1.0, 0.8, 0.7, 0.5, 0.38$ for $N = e^{\phi_0-\epsilon}(\phi_0-\epsilon)^{1/\alpha}$ and with (from top to bottom) $\alpha = 0.81, 0.8, 0.75, 0.6, 0.5, 0.38$ for $N = (\phi_0-\epsilon)^{1/\alpha}$. Solid squares represent the original $N = e^{\phi_0-\epsilon}(\phi_0-\epsilon)^{1/\alpha}$ and $N = (\phi_0-\epsilon)^{1/\alpha}$ distributions and open squares represent the distributions modified to be $N_{new} = N(1+\mu(\phi_0-\epsilon)^v)$. DARKexp with $\phi_0 = 2.55$ is plotted as the red data point for reference.

amplitude would be tied to asymptotic slope but this is only true for the energy distributions in equation (3.1) and equation (3.2) and not true for DARKexp.

To further test the idea of the oscillation's dependence on the steepness of the energy distribution slope, we altered $N = e^{\phi_0-\epsilon}(\phi_0-\epsilon)^{1/\alpha}$ and $N = (\phi_0-\epsilon)^{1/\alpha}$ by multiplying these energy distributions so that $N_{new} = N(1+\mu(\phi_0-\epsilon)^v)$ where N is the original distribution and μ and v are free parameters. The shape of the modification is arbitrary; we could have chosen a different modification. This resulted in the energy distribution having the same behavior near $\epsilon = \phi_0$ as the original distribution but a slightly steeper or shallower slope depending on the sign of μ and the normalization of the new distribution. We then calculated κ for both of the modifications and plotted them as open boxes alongside their counterparts in Figure 8 and Figure 9 for modifications with central potentials of $\phi_0 = 4.0$ and $\phi_0 = 2.55$, respectively.

Figures 7, 8, and 9 show that in general less negative $d\log(N)/d\epsilon$ lead to more pronounced oscillation in the density profile slope. However, $d\log(N)/d\epsilon$ is not an exact predictor of density slope oscillations: in Figures 8 and 9 a given value of $d\log(N)/d\epsilon$ corresponds to a range of values of κ. With more effort, it might be possible to devise a better predictor of density slope oscillations based on $N(E)$, but that is beyond the exploratory nature of the present paper. Furthermore, there are exceptions to our characterization shown in Figures

8 and 9: the shape of $N(\epsilon)$ of the Hernquist system [30] would predict that its density profile slope should show some oscillations, which is not the case. The corresponding point in Figure 9 is at approximately $(-1.25, 0)$.

4 Class 2: Density Slope Oscillations in Dynamically Evolved Halos

Here we show that density profiles of simulated and observed systems are well approximated by those obtained from modified DARKexp energy distributions. The modifications to DARKexp are small, implying that these simulated and observed systems are very close to being fully relaxed.

Our analysis implicitly assumes that the simulated and observed systems we consider here are the result of mostly collisionless relaxation. Here, the term collisionless applies to the gravitational aspect of the system's evolution, not to what its gas particles might be doing. To be gravitationally collisionless the potential must be smooth on the scale of the relevant particles. In the case of the centers of galaxies and clusters these particles are stars, and to make the potential grainy, and hence collisional, the number of stars must be considerably smaller than what these galaxies have. Hydrodynamic processes that operate in massive galaxies and clusters, including dissipation, may lead to "violent" potential fluctuations that can help drive collisionless relaxation. Therefore the evolution of both simulated pure dark matter halos, and massive observed systems can be considered collisionless.

4.1 Numerically simulated systems

The density profile of DARKexp with $\phi_0 \approx 4.0$ provides a good fit to the density profiles of the dark matter only simulations Via Lactea 2, GHALO [2], and Aquarius AQ-1 [33] as shown in the bottom panels of Figure 10. These simulations are high resolution and focus on halo central regions with the GHALO and Via Lactea 2 innermost resolved region being 0.05% of R_{vir} (120 pc) [2]. However, DARKexp is not a perfect match; there appear to be oscillations with higher frequencies in GHALO and Via Lactea 2 data, and at larger radii than the oscillations experienced in DARKexp density profiles. Aquarius AQ-1 does not appear to oscillate appreciably and is actually very well represented by DARKexp.

It is important to note that these oscillations are not the result of substructure. Substructure effects are subdominant to those of oscillations (if oscillations are present), as can be seen from published work. First, data from Stadel et al. [2], can be used to estimate the fractional density contained in oscillations in GHALO; it is about 10%. Oscillations are found around $r \sim 0.3 - 20$ kpc in their galaxy mass halo. Second, at the same range of radii, the cumulative fraction of mass in subhalos for a similar mass halo in the Aquarius simulation can be read off from Figure 12 of Springel et al. [33]. It is about 0.1%, or 100 times smaller than the mass contained in oscillations found in GHALO. Aquarius and GHALO are different simulations, but it is unlikely that they would differ by a factor of 100 in the fractional amount of mass in subhalos. Another possible reason for the oscillations are the streams from tidally disrupted subhalos. However, because the material from these is widely distributed throughout the halo, they are unlikely to be the dominant contributor to the oscillations.

We argue that oscillations in Via Lactea 2 and GHALO indicate that these systems are not fully relaxed. DARKexp assumes a relaxed, equilibrium system. This central assumption may not be fully realized in many physical systems where some mechanism may not be letting the system become fully relaxed. To try to mimic this effect, we modified DARKexp $N(\epsilon)$ with the goal of matching the observed density profile of these simulated halos. We used the

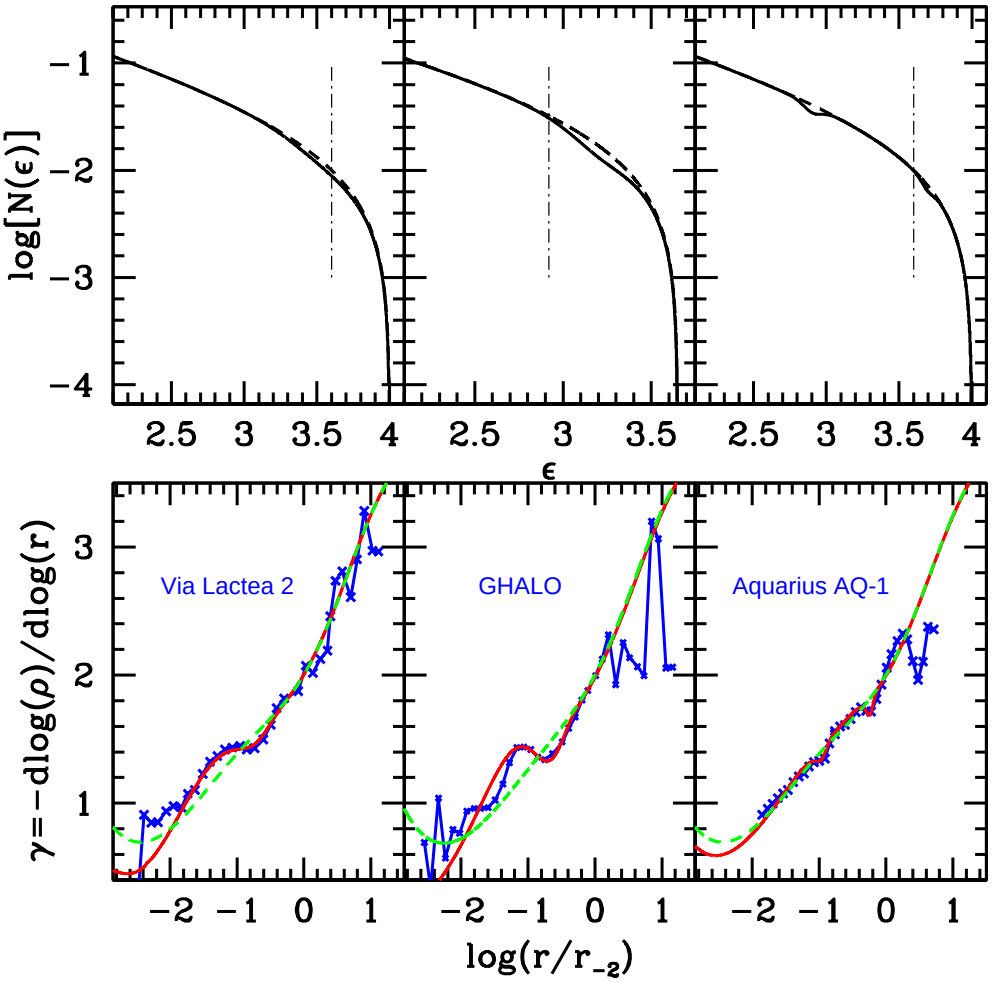

Figure 10. *Top panels* Energy distributions for Via Lactea 2 fit (left), GHALO fit (middle), and Aquarius AQ-1 fit (right) in solid lines plotted with DARKexp, dashed line, with the appropriate ϕ_0 where for Via Lactea $\phi_0 = 4.0$, GHALO $\phi_0 = 3.65$, and Aquarius AQ-1 $\phi_0 = 4.0$. The slight deviation is distinguishable at around $\epsilon = 0.8\phi_0$ where the two lines separate and a dashed-dot guideline is plotted at $\epsilon = 0.8\phi_0$ for reference. The difference between the two curves is a Gaussian peak and in the case of Aquarius AQ-1, two Gaussian peaks. The graph is zoomed in to this region to better show the difference between the curves and does not include the entire energy distribution. *Bottom panels* Density profile slopes for Via Lactea 2, GHALO, and Aquarius AQ-1 numerical simulations are plotted in blue and x symbols. The modified DARKexp that fits the data is plotted in red and the original DARKexp is plotted in green (dashed). The modified DARKexp distributions use the ϕ_0s listed above. In other words, the red line is a modified form of the green line. The bottom plots correspond to the plots directly above. The mass difference in the profile for $\log(r/r_{-2}) < 0$ between DARKexp and the modification is 0.58%, 0.56%, and 0.77% for Via Lactea 2, GHALO, and Aquarius AQ-1 respectively.

simplest profile modification: a small Gaussian peak was added to DARKexp. The new $N(\epsilon)$ is given by

$$N_{mod} = N + a \exp\left[-\frac{1}{2}\frac{(\epsilon - \bar{\epsilon})^2}{\sigma^2}\right] \tag{4.1}$$

where N is the standard DARKexp expression given by equation (2.1), a is a normalization scaling factor, and $\bar{\epsilon}$ and σ are the standard Gaussian parameters of average value and standard deviation, respectively. The modification can be seen in the top panel of Figure 10, where $\log[N(\epsilon)]$ is plotted for the original DARKexp energy distribution (dashed line) and the energy distribution modified from DARKexp that provide good fits to the density data (solid lines).

The corresponding density profiles are seen as red solid lines in the bottom panels of Figure 10, together with the data for Via Lactea 2 (left), GHALO (middle), and Aquarius AQ-1 (right), displayed as blue lines with crosses. Dashed green lines are the unmodified DARKexp profiles. In Via Lactea 2 and GHALO, this modification produced oscillations over two decades in radius with higher frequency than the oscillations found in the unmodified DARKexp profile, and at radii where unmodified DARKexp has a monotonically changing $\gamma(r)$ profile. The Aquarius modification, two very small Gaussian peaks added to DARKexp $N(\epsilon)$, did provide a better fit to the data then DARKexp alone but the Aquarius data does not oscillate like the Via Lactea 2 or GHALO data. The mass difference of the profiles for $\log(r/r_{-2}) < 0$ between the modified and unmodified DARKexp profiles with the same ϕ_0 is 0.58%, 0.56%, and 0.77% for Via Lactea 2 ($\phi_0 = 4.0$), GHALO ($\phi_0 = 3.65$), and Aquarius ($\phi_0 = 4.0$) respectively. This is a small difference confined to small radii. Again, one could imagine that in some systems, the oscillations will get averaged out by anisotropies or miscentering and spherical averaging. Likewise, it would not take much mass to create oscillations in this radius range, implying that these systems are very nearly, but not fully relaxed.

While we do not address the specific mechanisms leading to the small perturbation in the DARKexp energy distribution, we put forth one possibility. The systems which have $N(E)$ represented by the solid lines in the top panels of Figure 10 are prevented from achieving a fully relaxed state, represented by the dashed lines of the DARKexp $N(\epsilon)$. Because the number of particles increases rapidly with decreasing ϵ, it would take a very small number of particles with $\epsilon \lesssim 3$ (for Via Lactea 2) to fill in the 'hole' at $\epsilon \sim 3.5$. These particles would need to lose some energy and become more bound. What is holding them back? For example, small excess of angular momentum could create an angular momentum barrier preventing the particles from coming closer to the center of the halo and attaining lower energies. Such a scenario is not unlikely because, as discussed in Williams et al. [58] it is more difficult to redistribute angular momentum than energy, and so some particles may be stuck with their somewhat higher amount of angular momentum.

4.2 Observed systems

The observationally derived data taken from Newman et al. [19] provides density profiles for seven massive, equilibrium galaxy clusters seen in Figure 1. We transformed this data into the slope representation, γ, and plotted it in Figure 11 to better see the oscillations. All of the profiles possess oscillations in the central region. For reference, the density from a DARKexp profile with $\phi_0 = 4.0$ is also plotted. At large radii, the differences between DARKexp and the data arise because Newman et al. [19] dark matter component is approximated with a gNFW profile which has $\gamma = 3$ at large radii, while DARKexp asymptotes to $\gamma = 4$. We do not use the outer density profile in our analysis.

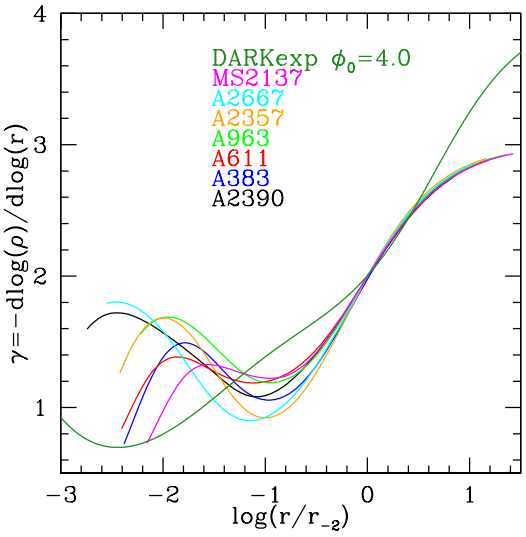

Figure 11. Density profile slopes for seven massive, equilibrium galaxy clusters presented in Newman et al. [19]. Oscillations are seen for all the profiles for $\log(r/r_{-2}) < 0$. DARKexp with $\phi_0 = 4.0$ is plotted for comparison. The Newman profiles asymptote to the outer slope of 3. The oscillations are higher frequency for the Newman profiles than DARKexp.

In addition to cluster total density profiles, we also use profiles of massive ellipticals, taken from Chae et al. [20], who carried out a comprehensive study of SDSS early type galaxies (ETGs) that also show density slope oscillations, or as they call them, S-shape profiles, at small radii. They used over 2,000 nearly spherical ETGs from SDSS coupled with empirical scaling relations to derive galaxy density profiles. The observational data for each galaxy consisted of its light profile and the velocity dispersion measured at $R_{\rm eff}/8$. The dark matter halos of galaxies were assumed to follow gNFW or Einasto profiles, each with three free parameters. These data and assumptions were supplemented with empirical scaling relations between $M_\odot$ and M_{200}, concentration and M_{200}, initial mass function (IMF) shape and the velocity dispersion, and velocity dispersion and the slope of the radially dependent velocity dispersion profile. The free parameters were fixed by requiring that the total density profile obey the Jeans equation. The authors present average density profiles for six separate total mass bins. We note that according to the Chae et al. [20] results, the amplitude of oscillations increases towards the higher galaxy mass bins. The oscillations in the density slopes of $M = 10^{14.5} M_\odot$ galaxies will be hard to fit with a small modification we use here. However, the overall nature of slope oscillations is the same for the whole range of galaxy masses presented in Chae et al. [20], from $M = 10^{12} M_\odot$ to $M = 10^{14.5} M_\odot$, so below we use just one representative mass range, $10^{13} M_\odot \pm 0.2$dex.

Since we are analyzing density slope oscillations, it is important to establish that cluster and galaxy data do indeed require oscillations to be present. Could one have instead fitted the data with a monotonically changing $\gamma(r)$ profile? Chae et al. [20] tried that approach, and found that single density profiles do not work (see their Section 4.2.1). In Figure 9, they plot the observed and single-profile predicted distributions of η, where $\sigma(R) \propto R^\eta$, is

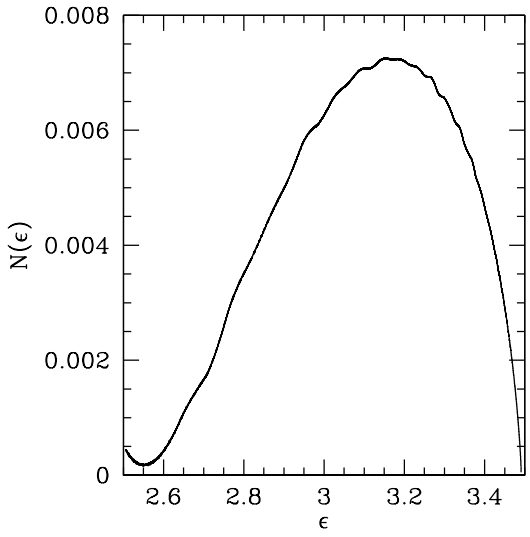

Figure 12. Difference between $N(E)$ derived from galaxy cluster Abell 611 (A611) density profile data and DARKexp $N(\epsilon)$ for $\phi_0 = 3.5$. The energy distribution for A611 is calculated from the density profile with a process outlined by Binney [54]. The peak is similar to a Gaussian, warranting the use of a Gaussian modification in this Section.

the luminosity weighted line of sight velocity dispersion within aperture R centered on the galaxy. The data gives $\langle\eta\rangle = -0.06 \pm 0.01$, while fitting a single gNFW yields $\langle\eta\rangle = -0.01$, or 5σ away from the observed mean. Newman et al. [19] do not fit single profile models, but point out that the stellar mass of the central elliptical is significant at radii $\lesssim 5$ kpc, often leading to the steepening of the central profile slope. We conclude that for cluster and galaxy total density profiles, single-profile models are statistically disfavored and hence, density slope oscillations are indicated by the data.

We chose two galaxy clusters from Newman et al. [19], A963 and A611, and one galaxy mass range from Chae et al. [20], $10^{13}M_\odot \pm 0.2$dex. The unmodified DARKexp (dotted) and modified (dashed) $N(\epsilon)$ are shown in Figure 13 with green, red, and black lines respectively. The corresponding modified $\gamma(r)$ profiles are the dashed lines in Figure 14, shown together with the data (solid lines). For fitting purposes, we only used data where $\log(r/r_{-2}) < 0$ since DARKexp and the data have different large radius asymptotic behavior, as discussed above.

In all the fits, the introduction of a Gaussian modification to $N(\epsilon)$ modified DARKexp density profiles such that these now fit the frequency and amplitude of the observed data. The mass difference in the profiles at $\log(r/r_{-2}) < 0$ between the modified and their original DARKexp profiles is 2.0%, 2.52%, and 19.1% for A611, A963, and $M_{gal} = 10^{13}M_\odot$ galaxies bin, respectively. It is likely that the percentages are related to the location of the Gaussian peak as the fit modification for the Chae et al. galaxies' profile was different than the other fits. This is because its Gaussian peak was located at $\epsilon = 0.34\phi_0$ whereas the others are closer to $\epsilon = 0.85\phi_0$.

To check if the Gaussian shape provides a reasonable approximation to the difference

between the energy distributions of DARKexp and the data, we calculated the shape of the actual difference between $N(E)$ derived from galaxy cluster A611 density profile and DARKexp $N(\epsilon)$ with $\phi_0 = 3.5$. The result is a skewed peak shown in Figure 12. (We calculated the energy distribution of A611 from its density profile with an algorithm outlined by Binney [54].) The peak is similar enough to a Gaussian to warrant the use of equation (4.1).

We emphasize that the modifications added to DARKexp $N(\epsilon)$ to reproduce simulated halos and observed systems are the same, both given by equation (4.1). This suggests that both types of systems share the same characteristic, which we argue is their state of incomplete relaxation in the central regions. The fact that the amplitude of modification is smaller in the case of simulated halos (top panels of Figure 10) than observed systems (Figure 13) argues that the former are closer to being fully relaxed that the latter.

We note that the modifications we added to DARKexp in this Section are consistent with our findings in Section 3: making the $N(\epsilon)$ slope less negative around $\epsilon = 0.8\phi_0$ results in greater density slope oscillations in the corresponding density profiles.

We also note that there may be some degeneracy between the Gaussian parameters a, $\bar{\epsilon}$ and σ (equation (4.1)) and the starting central potential ϕ_0, when fitting the density profiles. Solutions may not be unique as one set of parameters with a central potential can give similar results to another central potential with different modification parameters.

5 Conclusions

As we show in this paper, many, if not most of these systems exhibit non-monotonic changes in slope, or oscillations. Galaxies and clusters, whether observed or simulated can be described collectively as dynamically evolved because they are the result of evolution, either in the real universe, or in a computer. Monotonically changing density profile slopes appear to be the exception rather than the rule in the very central regions of observed and simulated galaxies and clusters, and pure dark matter halos.

Oscillations are also common in other types of systems, those that were arrived at starting from a distribution function of a differential energy distribution, such as the isothermal sphere and DARKexp. Systems that do not have slope oscillations are mostly those that were constructed that way: NFW, Einasto, Hernquist, etc.

In this paper, we study the two classes of systems whose profile slopes do oscillate: systems based on a physical principle or derivation (Class 1), and expressed in terms of $f(E)$ or $N(E)$; we call these physics-based, and dynamically evolved systems (Class 2). The two types of oscillations appear to be unrelated, and can be superimposed in a single system. Slope oscillations in the dynamically evolved systems occur at $-2 \lesssim \log(r/r_{-2}) \lesssim 0$, while those in the relaxed, collisionless, physics-based systems (DARKexp) start at smaller radii, $\log(r/r_{-2}) \lesssim -2$.

We argue that slope oscillations in the dynamically evolved systems occur because these systems are not fully relaxed. To support our claim, we show that adding a small perturbation to the $N(E)$ of a fully relaxed system, namely DARKexp, reproduces the oscillating density profiles of observed and simulated systems. The fact that the modifications to $N(E)$ are small and affect a small fraction of the systems' energy distribution implies that these systems are close to being fully relaxed.

Non-monotonically changing density slopes (or oscillations) in physics-based systems have a different origin. It appears that a generic monotonically changing $f(E)$ or $N(E)$ does not produce a monotonically changing density slope. This conclusion is based on the behavior

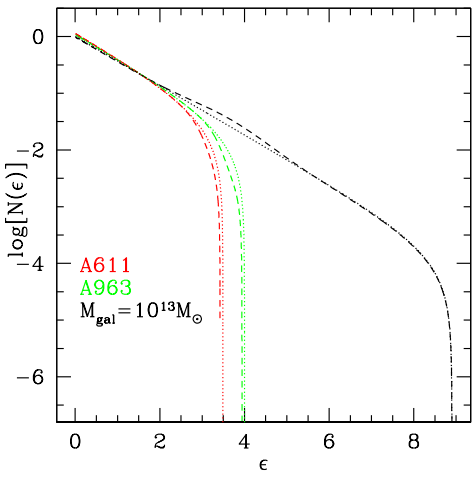

Figure 13. Energy distributions of the modified DARKexp profiles (dashed) plotted against their original DARKexp profiles (dotted) with $\phi_0 = 3.5$, $\phi_0 = 4.0$, and $\phi_0 = 8.9$. The deviations from DARKexp are distinguishable at around 85% of ϕ_0 for A611 and A963 whereas the peak for the Gaussian for the Chae et al. [20] $M_{gal} = 10^{13} M_\odot$ modification is found at 35% of ϕ_0. The modified DARKexp profiles provide fits to the density profiles plotted in Figure 14.

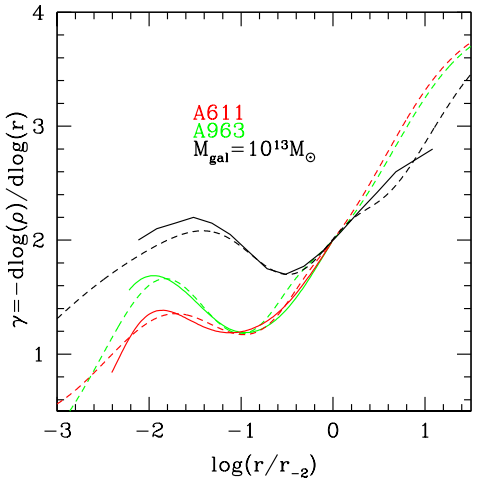

Figure 14. Density profile slopes for three profiles (solid lines), one taken from Chae et al. [20] and two from Newman et al. [19], and their best fit formed from modifying DARKexp with a Gaussian (dashed lines). The mass difference in the profiles at $\log(r/r_{-2}) < 0$ between DARKexp and the modification is 2.0%, 2.52%, and 19.1% for Newman et al. [19] A611, A963 and Chae et al. [20] $10^{13} M_\odot$ respectively. The modified profiles (dashed) are the density profiles that correspond to the modified DARKexp energy distributions found in Figure 13.

of the systems like isothermal spheres, King profiles, certain polytropes, and DARKexp, as well as our (limited) exploration of other functional forms for $N(E)$. We are not claiming that all physics-based systems show density slope oscillation, but only that these are common. Focusing on the density slope oscillations at small radii, we then ask if the magnitude of these oscillations can be predicted solely from the shape of the corresponding $N(E)$. We devise a metric to quantify density slope oscillations, and show that it is related to a property of $N(E)$, namely $d\log(N)/d\epsilon$ measured at $\epsilon = 0.8\phi_0$. While the relation between the two has some scatter, it does confirm our claim that density slope oscillations are the consequence of the shape of $N(E)$.

The most interesting avenue for future work is to further investigate the dynamically evolved systems (Class 2). We plan to investigate the time evolution of simulated systems with the goal of measuring how $N(E)$ evolves over time and what corresponding effects this has on the density profile for halos. For the simulated systems, where everything is known about the constituent particles, it is possible to obtain the system's actual $N(E)$, instead of calculating it from the density profile, as we have done here. If the deviation of the $N(E)$ from that of the relaxed DARKexp is indeed a small deficit of particles, localized in energy, then it would be interesting to investigate why the system did not attain full relaxation. Was

it that the particles were not able to freely exchange angular momentum during evolution, as we speculate, or something else? If it is, for example, angular momentum, then the similarity between density slope oscillations in simulated and observed systems (see Fig. 10 and 14) suggests that the two types of systems have similarities in their distributions of angular momentum. This information can give us a new tool to understand the dynamics within the observed galaxies and clusters, and add to the current tool kit which consists of mass distribution obtained from lensing and line of sight velocity dispersion(s), or velocity distributions.

More generally, by comparing a system's properties, and especially $N(E)$, to those of DARKexp, one can better ascertain a system's dynamical state. Recall the hierarchy of states that a self-gravitating system can find itself in. Fully relaxed is not the same as virialized, or being in Jeans (hydrostatic) equilibrium. A virialized system possesses some global, or integral properties, but need not satisfy anything else. Jeans equilibrium implies more than just the virial equilibrium, but it does not, strictly speaking, guarantee that the system is even stable. Most galaxies and clusters, real and simulated, that have a smooth circular/spherical or elliptical appearance over some prolonged period of time are likely in stable Jeans equilibrium. But even that does not mean that they are fully relaxed. The state of full relaxation means that the system is not only in a long term stable equilibrium, but that it has also erased its formation and evolution history. While determining if a system is in stable Jeans equilibrium is relatively easy (in simulations and observations), it is difficult to know if it is relaxed. Comparison to DARKexp, a theoretically derived collisionlessly relaxed model, might be the best way to establish that.

Acknowledgments

We thank Andrew Newman for sharing their data on galaxy clusters, and Andrew Newman and Kyu-Hyun Chae for answering our questions about their work over email.

References

[1] Navarro, J. F., Hayashi, E., Power, C., Jenkins, A. R., Frenk, C. S., White, S. D. M., Springel, V., Quinn, T. R., 2004, MNRAS, 349, 1039

[2] Stadel, J., Potter, D., Moore, B., Diemand, J., Madau, P., Zemp, M., Kuhlen, M., Quilis, V., 2009, MNRAS, 398, L21.

[3] Navarro, J. F., Frenk, C. S., & White, S. D. M. 1997, ApJ, 490, 493

[4] Diemand, J., Zemp, M., & Stadel, J. 2004, MNRAS, 353, 624

[5] –. 2005a, Nature, 433, 389

[6] Diemand, J., Zemp, M., Moore, B., Stadel, J., & Carollo, C. M. 2005b, MNRAS, 364, 665

[7] Diemand, J. & Moore, B. 2011, Advanced Science Letters, 4, 297

[8] Ludlow, A. D., Navarro, J. F., White, S. D. M., Boylan-Kolchin, M., Springel, V., Jenkins, A., & Frenk, C. S. 2011, MNRAS, 415, 3895

[9] Navarro, J. F., Hayashi, E., Power, C., Jenkins, A. R., Frenk, C. S., White, S. D. M., Springel, V., Quinn, T. R., 2010, MNRAS, 402, 21

[10] Tasitsiomi, A., Kravtsov, A. V., Gottlöber, S., & Klypin, A. A. 2004, ApJ, 607, 125

[11] Flores, R. A., & Primack, J. R. 1994, ApJL, 427, L1

[12] Dubinksi, J., & Carlberg, R. G. 1991, ApJ, 378, 496

[13] Pontzen, A. & Governato, F. 2014, Nature, 506, 171

[14] Weinberg, D. H., Bullock, J. S., Governato, F., Kuzio de Naray, R., & Peter, A. H. G. PNAS, 2015: 1308716112v1-201308716.

[15] Remus., RS., Burkert, A., Dolag, K., Johansson, P. H., Naab, T., Oser, L., Thomas, J., 2013, ApJ, 766, 2

[16] Diemand, J., Kuhlen, M., Madau, P., Zemp, M., Moore, B., Potter, D., & Stadel, J. 2008, Nature, 454, 735

[17] Merritt, D., 2009, ApJ, 694, 959

[18] Böker, T., et al. 2002, AJ, 123, 1389

[19] Newman, A. B., Treu. T., Ellis R. S., Sand, D. J., Nipoti, C., Richard, J., Jullo, E. ApJ 765 24

[20] Chae, K., Bernardi, M., Kravtsov, A.V., 2013, MNRAS, 437, 3670

[21] Tal, T., Wake, D. A., & van Dokkum, P. G., 2012, ApJL 751, L5

[22] Williams, L. L. R., Hjorth, J., 2010, ApJ, 722, 856

[23] Hjorth, J., Williams, L. L. R. 2010, ApJ, 722, 851

[24] Féron, C., Hjorth J., 2008, Phys. Rev. E 77, 022106

[25] Medvedev, M. V., Rybicki, G., ApJ, 555, 863

[26] Binney, J., Tremaine, S., 1987. Galactic Dynamics (1st ed.; Princeton NJ: Princeton Univ. Press)

[27] Gieles, M. & Zocchi, A. 2015, ArXiv e-prints, 1508.02120

[28] King, I. R. 1966, Astro. J., 71, 64

[29] Schaya, J., et al. 2015, MNRAS, 446, 521

[30] Hernquist, L. 1990. ApJ, 356, 359

[31] Einasto, J., 1965, Trudy Astrofizicheskogo Instituta Alma-Ata, 5, 87

[32] Boylan-Kolchin, M., Springel, V., White, S. D. M., Jenkins, A., Lemson, G. 2009, MNRAS, 398, 1150

[33] Springel, V., Wang, J., Vogelsberger, M., Lodlow, A., Jenkins, A., Helmi, A., Navarro, J. F., Frenk, C. S., White, S. D. M., 2008 MNRAS, 391, 1685

[34] Gnedin, O. Y., & Zhao, H. 2002, MNRAS, 333, 299

[35] Mashchenko, S., Wadsley, J., Couchman, H. M. P. 2008, Science, 319, 174

[36] Navarro, J. F., Eke, V. R., Frenk, C. S. 1996, MNRAS, 283, L72

[37] Nipoti, C., Binney, J. 2015, MNRAS, 446, 1820

[38] Oñorbe, J., et al. 2015, ArXiv e-prints, 1502.02036

[39] Pontzen, A. & Governato, F. 2012, MNRAS, 421, 3464

[40] Read, J. I., & Gilmore, G. 2005, MNRAS, 356, 107

[41] Read, J. I., Agertz, O., Collins, M. L. M. 2015 eprint arXiv:1508.04143

[42] Teyssier, R., Pontzen, A., Dubois, Y., Read, J. I. 2013, MNRAS, 429, 3068

[43] El-Zant, A., Shlosman, I., Hoffman, Y., 2001, ApJ, 560, 636

[44] Brook, C. B., et al. 2012, MNRAS, 426, 690

[45] Cusworth, S. J., Kay, K. T., Battye, R. A., & Thomas, P. A. 2014, MNRAS, 439, 2485

[46] Di Cintio, A., Brook, C. B., Dutton, A. A., Macciò, A. V., Stinson, G. S., Knebe, A. 2014, MNRAS, 441, 2986

[47] Duffy, A. R., Schaye, J., Kay, S. T., Dalla Vecchia, C., Battye, R. A., & Booth, C. M. 2010, MNRAS, 405, 2161

[48] Gnedin, O. Y., Kravtsov, A. V., Klypin, A. A., & Nagai, D. 204, ApJ, 616, 16

[49] Pedrosa, S., Tissera, P. B., & Scannapieco, C. 2009, MNRAS, 295, L57

[50] Sawala, T., Frenk, C. S., Crain, R. A., Jenkins, A., Schaye, J., Theuns, T., & Zavala, J. 2013 MNRAS, 431, 1366

[51] Sawala, T., et al. 2015, MNRAS, 448, 2941

[52] Schaller, M., Frenk, C. S., Bower, R. G., Theuns, T., Jenkins, A., Schaye, J., Crain, R. A., Furlong, M., Vecchia, C. D., McCarthy, I. G., 2015, MNRAS, 451, 1247

[53] Velliscig, M., van Daalen, M. P., Schaye, J., McCarthy, I. G., Cacciato, M., Le Brun, A. M. C., & Vecchia C. D. 2014, MNRAS, 442, 2641

[54] Binney, J. 1982, MNRAS, 200, 951

[55] Beraldo e Silva, L. J., Lima, M., & Sodré L. 2013, MNRAS, 436, 2616.

[56] Hjorth, J., Williams, L. L. R., Wojtak, R., & McLaughlin, M., 2015, ApJ, 811, 1, 2

[57] Umetsu, K., Zitrin, A., Gruen, D., Merten, J., Donahue, M., Postman, M., ApJ, accepted

[58] Williams, L. L. R., Hjorth, J., Wojtak, R., 2014, ApJ, 783, 13

[59] Nolting, C., Williams, L. L. R., Boylan-Kolchin, M., & Hjorth, J., 2016, JCAP, submitted